

Alaska megathrust 1: Seismicity 43 years after the great 1964 Alaska megathrust earthquake

Jiyao Li,^{1,2} Geoffrey A. Abers,¹ YoungHee Kim,^{1,3} and Douglas Christensen⁴

Received 7 May 2013; revised 20 August 2013; accepted 27 August 2013; published 16 September 2013.

[1] The largest moment release during the 1964 Mw 9.2 Alaska earthquake was on the portion of the megathrust under the eastern Kenai Peninsula and the Prince William Sound. The area is currently locked geodetically and corresponds to where the Yakutat terrane is subducting. In 2006–2009, a seismic array consisting of 34 broadband seismometers was deployed in the region. An automatic algorithm was used to detect 12,563 local earthquakes using 13 months of data from the experiment. Of these, 9427 good quality earthquakes could be relocated in a joint inversion for hypocenters and velocity structure. They were then relocated by double difference to generate a final catalog of 8308 hypocenters. These microearthquakes delineate a deeper steeply dipping Wadati-Benioff zone contiguous with an 11 km wide seismic zone dipping at 3° between 20 km and 40 km depth along the 1964 earthquake's rupture zone. Focal mechanisms do not show interplate thrust faulting events, but mostly normal faulting events with T axes generally parallel the slab dip direction, indicating them to be intraslab seismicity. The shallow narrow band of seismicity lies within the subducting Yakutat terrane and right below the thrust zone. Possibly, thrust faulting has not yet resumed yet in this early phase of the earthquake cycle. Thick subducted sediments overlying the Yakutat terrane could also form a large strong contact zone on a relatively smooth plate boundary, which does not favor seismic sliding on small patches but ruptures homogenously in great earthquakes.

Citation: Li, J., G. A. Abers, Y. H. Kim, and D. Christensen (2013), Alaska megathrust 1: Seismicity 43 years after the great 1964 Alaska megathrust earthquake, *J. Geophys. Res. Solid Earth*, 118, 4861–4871, doi:10.1002/jgrb.50358.

1. Introduction

[2] The largest earthquakes, with magnitudes greater than 8, mostly occur on the megathrust in the seismogenic part of subduction zones [Pacheco and Sykes, 1992]. These great megathrust earthquakes are relatively infrequent, separated by long aseismic intervals. Even during the intervals between $Mw > 8$ earthquakes, abundant small-to-medium seismicity occurs [e.g., Byrne *et al.*, 1988; Tichelaar and Ruff, 1993]. Although most subduction zones show small to moderate interplate thrust earthquakes [e.g., Igarashi *et al.*, 2003;

Pacheco *et al.*, 1993; Zhang and Schwartz, 1992], a few show only seismicity within the downgoing slab, not on the plate interface, even at megathrust depths [e.g., Taber and Smith, 1985; Dzierma *et al.*, 2012]. The different patterns of seismic behavior could reflect different levels of material heterogeneity on megathrust, manifest as long-lived asperities [Lay *et al.*, 1982; Lay and Bilek, 2007; Thatcher, 1990]. By “asperity,” we mean a patch on a fault with relatively high moment release. Alternatively, it is possible that the seismicity behavior varies with time in the seismic cycle, as it does in the outer rise and downdip of the thrust zone [Christensen and Ruff, 1988; Lay *et al.*, 1989].

[3] The 27 March 1964 Alaska “Good Friday” earthquake (Mw 9.2), one of the largest three earthquakes recorded, ruptured from north of Prince William Sound (PWS) westward for 600–800 km along strike to the western side of Kodiak Island (Figure 1) [Plafker, 1965]. A large area of the PWS and the eastern Kenai Peninsula slipped ~25 m coseismically, releasing most of the seismic moment, and is referred to as the “PWS asperity” [Christensen and Beck, 1994; Ichinose *et al.*, 2007]. GPS observations also show a strong interplate locking area with the same location as the large rupture asperity of the 1964 earthquake [Suito and Freymueller, 2009; Zweck *et al.*, 2002]. North of the PWS asperity, a slow slip event took place from 1998 to 2001 downdip of the locked zone [Ohta *et al.*, 2006], but otherwise no large thrust events have occurred since 1964. The estimated recurrence interval of major earthquakes in this region ranges from 333 to

This article was originally published on September 16, 2013. Subsequently, additional author alterations and a correction to the order of figures were made. The corrected version was published online on 16 September 2013.

Additional supporting information may be found in the online version of this article.

¹Lamont-Doherty Earth Observatory of Columbia University, Palisades, New York, USA.

²Department of Earth and Environmental Sciences, Columbia University, New York, USA.

³School of Earth and Environmental Sciences, Seoul National University, Seoul, South Korea.

⁴Geophysical Institute, University of Alaska Fairbanks, Fairbanks, Alaska, USA.

Corresponding author: J. Li, Lamont-Doherty Earth Observatory of Columbia University, 61 Route 9W, Palisades, NY 10964, USA.
(jiyao@ldeo.columbia.edu)

©2013. American Geophysical Union. All Rights Reserved.
2169-9313/13/10.1002/jgrb.50358

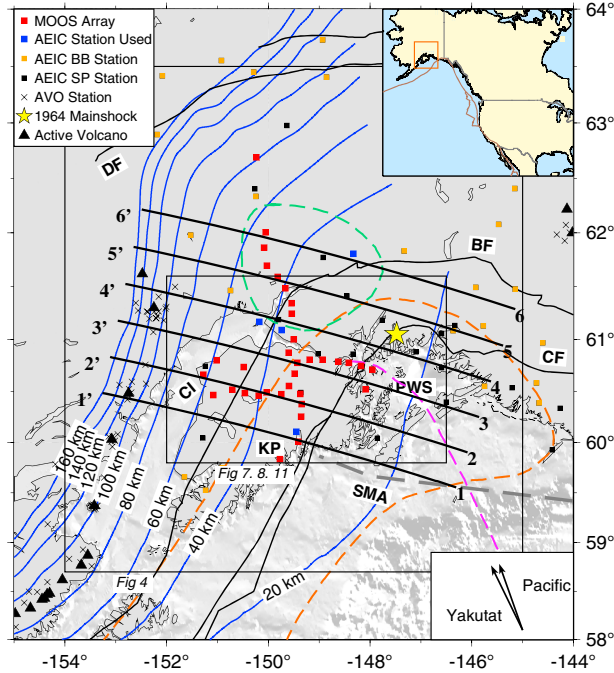


Figure 1. Map of south-central Alaska showing MOOS array (red squares), AEIC broadband stations used (blue squares), other AEIC broadband stations (orange squares), AEIC short period stations (black squares), and AVO stations (black crosses). Thick, equidistant black lines are projection lines for cross sections. Thin, irregular black lines represent major faults: BF, Border Ranger Fault; CF, Contact Fault; DF, Denali Fault. Gray dashed line is the Slope Magnetic Anomaly (SMA). Blue lines indicate the plate interface depth contours based on this study. Green dashed line marks the slow slip event region [Ohta et al., 2006]. Pink dashed line shows the offshore refraction survey line (TACT) [Brocher et al., 1994]. Orange dashed line denotes the 1964 PWS earthquake rupture zone. KP: Kenai Peninsula; CI: Cook Inlet; PWS: Prince Williams Sound.

875 years [Carver and Plafker, 2008]. Thus, at present, this megathrust is still early in the earthquake cycle, and small thrust faulting earthquakes seem rare.

[4] This paper reports results from the first campaign seismicity study in the region since the great 1964 earthquake. The 1964 Mw 9.2 earthquake ruptured in part beneath land areas of Kodiak and the Kenai Peninsula, which overlie the thrust zone. This geography allows the deployment of seismometers directly above the seismogenic zone, in an array that can detect and precisely locate seismicity below magnitude 1.0 and determine many well-constrained focal mechanisms. While seismicity is very well localized in a narrow band, none of the mechanisms show thrust faulting, and the earthquakes lie within the downgoing plate. Thus, even though the plate boundary has ruptured in great earthquakes and clearly exhibits frictionally unstable behavior, conditions are not favorable for small earthquake nucleation at present.

1.1. Tectonic Setting

[5] South Alaska has been formed by accretion of a series of exotic terranes originating far to the south since Cretaceous [Plafker et al., 1994]. Most recently, the Yakutat terrane

impinged on the North American continent about 6 Ma ago [Bruns, 1983] and continues to converge at rates close to the Pacific plate velocity [Elliott et al., 2010]. Ferris et al. [2003] revealed unusually thick (14–20 km) crust subducting down to 130 km depth northwest of the Kenai Peninsula, inferred to be the deeper subducting continuation of the Yakutat crust. The Slope Magnetic Anomaly [Griscom and Sauer, 1990] and seismic tomography [Eberhart-Phillips et al., 2006] also indicate that the Yakutat terrane lies under PWS and Kenai Peninsula. From a nearby refraction seismic transect, Brocher et al. [1994] suggest that the Yakutat terrane consists of oceanic crust overlying Pacific crust with intervening sediments, making a ~15 km thick composite layer subducting under PWS region. However, more recent study shows a single subducting layer of the Yakutat with 15–30 km thickness further southeast [Worthington et al., 2012]. These observations indicate that the shallow portion of the Yakutat terrane coincides with the PWS asperity and may control it.

[6] Previous studies have clearly delineated a continuous band of Wadati-Benioff Zone (WBZ) seismicity dipping northwest down to 150–200 km in the Cook Inlet region, showing the geometry of the subducting slab [e.g., Doser and Veilleux, 2009; Page et al., 1989; Ratchkovski and Hansen, 2002]. (In this paper, we refer to the WBZ to include all earthquakes within the downgoing plate, including those adjacent to the thrust zone.) Abundant shallow seismicity also exists in the strongly locked region. Downdip of the 1964 earthquake rupture zone, focal mechanisms show complex patterns consistent with downdip extension [Lu et al., 1997; Veilleux and Doser, 2007]. However, due to the scattering of the shallow seismicity and scant focal mechanisms, it is hard to relate the seismicity to the megathrust fault unambiguously. The complex regional tectonics also complicates understanding where the megathrust fault lies.

2. Data and Methods

2.1. Data

[7] The MOOS (Multidisciplinary Observations Of Subduction) project deployed a dense temporary seismic network on the Kenai Peninsula from May 2006 to June 2009 (Figure 1). At its peak, 34 broadband seismometers from IRIS-PASSCAL instrument center were in simultaneous operation for 13 months from August 2007 to August 2008. In this study, we only use data from the time period of full network operation. The stations were spaced 10–15 km apart (Figure 1) and recorded at 50 samples per second.

[8] A sequence of automatic earthquake detection and picking methods were used to locate all possible events. First, we calculated a short time average (1 s) to long time average (10 s) ratio of seismic energy (STA/LTA) [Allen, 1978] on each vertical trace filtered at 2–8 Hz, to detect all possible signals. If more than eight traces produced detections within a 20 s time window, this was regarded as a candidate event. A subsequent grid search tested each associated event against possible hypocenters in area within 154°W–146°W longitude and 58.5°N–63°N latitude, calculating theoretical P and S travel times with the *iasp91* velocity model [Kennett and Engdahl, 1991] and comparing them with the detections. This procedure detected and associated 16,462 events in 13 months. We manually reviewed them to eliminate obvious nonlocal earthquake signals, distant earthquakes far away

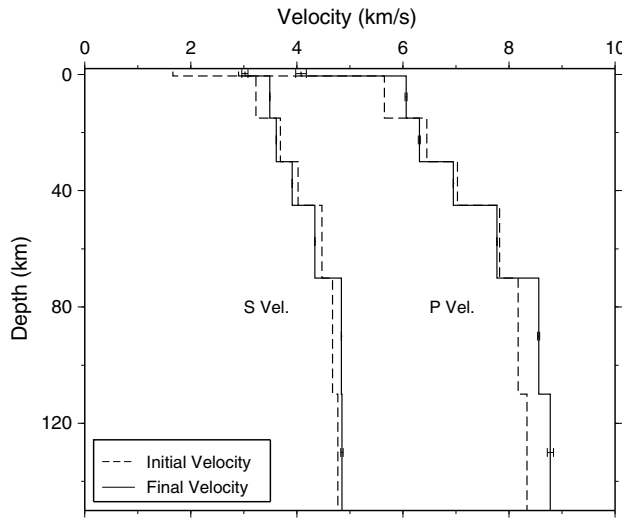


Figure 2. Initial and final 1D velocities for P and S waves. Formal (2-sigma) errors of final velocity model are shown in error bars.

from the network, noise and potential glacial-related signals, leaving 12,480 local earthquakes.

[9] Next, picks were refined and additional picks added. The acausal signals produced by finite impulse response (FIR) filters were corrected to minimum phase, to correct and sharpen signal onsets [Scherbaum and Bouin, 1997]. Onsets and uncertainties were then estimated with an adaptive autoregressive onset estimation algorithm [Pisarenko *et al.*, 1987]. This approach gives more precise estimation of P arrivals for low signal-to-noise levels and is much more capable of identifying S arrivals compared to the STA/LTA detector. In total, 269,606 P-arrival and 304,289 S-arrival times were produced this way. However, since arrivals were picked on each station independently, there are still many false picks especially when SNR is lower than 3. Based on preliminary locations from a grid search, we remove as outliers P arrivals more than 1.5 s and S arrivals with more than 2.0 s from the predicted arrivals, keeping 230,539 P and 203,792 S picks.

2.2. Earthquake Location

[10] The grid search method gives a starting hypocenter of each event, for subsequent steps of relocation. We apply two steps for earthquake relocation: single event location to improve all hypocenters while determining velocities and assessing absolute location uncertainties, and double difference earthquake location to increase precision. Initial locations use velocities averaged from the 1-D model of *Eberhart-Phillips et al.* [2006]. After initially relocating all events and sorting them based on stability, a subset of 3921 events were chosen for the single-event joint inversion. These events fit requirement that (1) hypocenter condition numbers (the ratio of the largest to smallest eigenvalues in the hypocentral inversion problem) < 50 , (2) rms residuals 0.5 s, (3) the changes in last step of iteration < 2 km, (4) the total changes in hypocenters < 50 km, (5) standard errors in hypocenters < 3 km, and (6) at least 11 stations recorded at least four S phases and more P phases than S phases. We conduct inversion for both earthquake hypocenter and 1D velocity model following *Abers and Roecker* [1991]. A parameter

separation technique [*Pavlis and Booker*, 1980] was used to decouple earthquake location and velocity inversion steps.

[11] The inversion for velocity and hypocenter is iterated until the changes in global residual variance and velocity are less than 1–2%, in practice seven times. Station corrections were calculated as the mean travel time residual at each station after four inversions and included in later iterations, resulting in 33% improvement in residual variance. The final velocity model (Figure 2 and Table 2) with station corrections (Table 1) ultimately reduces residual variance by 40% from the starting model and is used to relocate all the events. The final velocity layers, except for the top near-surface one, have resolution diagonals > 0.98 and formal error (2σ) < 0.06 km/s. In this model, all earthquakes are relocated and retested for stability; a total of 9247 relocated events meet stability criteria. For that larger catalog, we further improve the precision of earthquake location by using the double difference hypocenter location (hypoDD) [*Waldauser and Ellsworth*, 2000], to relocate earthquakes relative to one another. We were able to relocate 8308 events via hypoDD.

[12] Figure 3 shows hypocenters projected along one cross section from three different steps in the relocation procedure: the grid-search initial locations, single-event relocations, and

Table 1. Station Information

Station Name	Latitude (°)	Longitude (°)	Elevation (m)	Station Correction for P Arrival (s)	Station Correction for S Arrival (s)
BING	60.5169	-150.7040	89	0.07	0.50
PORT	60.8049	-148.9316	43	0.32	0.74
HOPJ	60.7760	-149.4255	221	0.18	0.11
NANC	61.6954	-150.0294	125	-0.15	-0.16
aval	60.3755	-149.3468	222	0.06	0.11
USKI	60.4601	-150.1900	127	-0.18	-0.42
SOLD	60.4641	-151.0815	116	0.03	0.35
WHIT	60.7866	-148.6238	81	0.01	-0.08
HOPE	60.8738	-149.5977	498	0.00	-0.05
HOLG	59.8351	-149.7697	46	0.02	-0.07
MAIN	60.5183	-148.0914	44	-0.07	0.02
PERI	60.7098	-147.9534	65	-0.10	0.29
CLRS	60.7458	-148.1780	50	-0.03	0.08
HEAD	60.0084	-149.4095	55	-0.08	-0.11
INDI	61.0010	-149.4979	127	0.12	0.02
MCDC	61.3427	-149.5454	162	-0.03	-0.21
DEVL	60.5508	-149.5941	306	0.04	-0.09
CASW	62.0056	-150.0535	106	-0.07	-0.12
LSUM	60.6717	-149.4810	446	0.05	-0.12
SNUG	60.4731	-149.7468	191	0.30	0.47
TUPA	60.8045	-149.1872	344	0.06	-0.08
RUSS	60.4881	-150.0316	150	-0.00	-0.14
MOOP	60.4754	-149.3739	242	0.11	0.15
DIVI	60.2564	-149.3559	273	0.03	0.09
LSKI	60.4832	-150.4617	116	-0.28	-0.19
MPEN	60.7352	-150.4823	130	0.22	0.68
ALPI	61.2448	-149.5397	811	-0.10	-0.23
COOK	60.7990	-151.0176	40	0.10	0.37
NSKI	60.6622	-151.2770	60	-0.13	0.37
BLAK	60.7746	-148.4171	46	-0.03	-0.04
BIGB	61.5919	-149.8174	91	0.26	0.64
KASH	61.8636	-150.0817	100	-0.08	0.03
KNIK	61.4859	-149.6688	65	0.25	0.60
BYR	62.6892	-150.2320	402	0.17	-0.00
FIB (AEIC)	61.1662	-150.1753	62	0.29	0.70
RC01 (AEIC)	61.0896	-149.7368	383	-0.21	-0.21
SAW (AEIC)	61.8076	-148.3295	782	-0.10	-0.09
SWD (AEIC)	60.1049	-149.4507	68	0.05	0.10

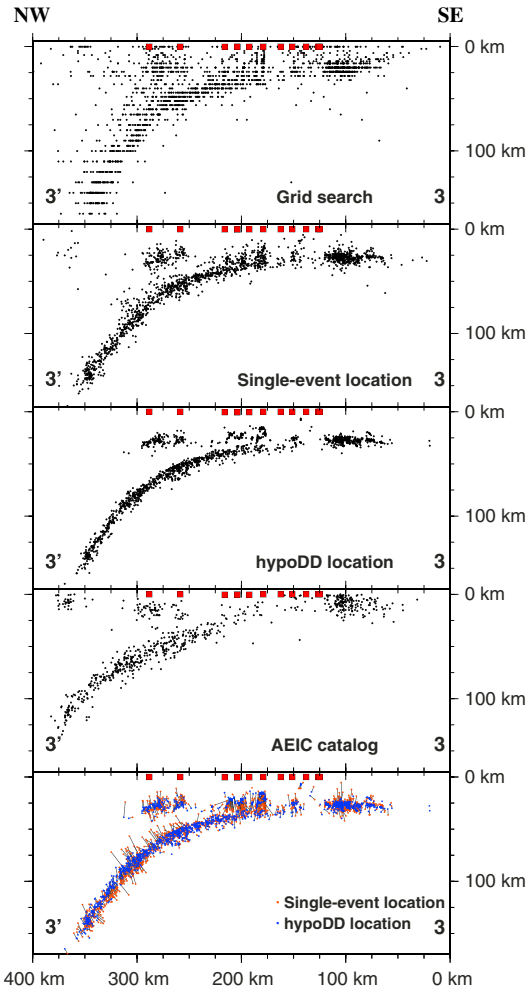


Figure 3. Seismicity located by different methods projected on cross-section line 3-3' within 20 km distance. (a) Grid search initial locations; (b) Single-event relocations; (c) hypoDD relocations; (d) AEIC catalog locations for the same period; (e) The movement of hypocenters from single-event locations to hypoDD locations, as indicated. Red squares show the MOOS stations.

the hypoDD hypocenters, along with the standard AEIC catalog for the same period. The initial locations show that shallower earthquakes (depth <40 km) scatter almost everywhere but the deeper seismicity roughly delineates a downgoing slab dipping to the west. The relocated single-event locations show the shape of downgoing slab from 20 km to 150 km depth but subducting seismicity still scatters within a 17 km wide band that holds 90% of the seismicity. Earthquakes relocated by hypoDD are more concentrated in a narrow WBZ, or in upper plate clusters. Seismicity in the downgoing slab narrows down to a 9.4 km wide band containing 90% of the seismicity. As comparison, earthquakes from AEIC catalog also show a 20 km wide downgoing WBZ but depths are overall shallower than the earthquake recorded by MOOS array and there are $\sim 50\%$ fewer earthquakes reported for the same time period. Seismicity from AEIC catalog is diffuse at shallower depth (<40 km) and the thrust zone cannot be identified, owing to the sparse (40–60 km spacing) AEIC network in the region (Figure 1). Compared with single-event locations

(Figure 3e), 48.5% of hypoDD hypocenters move down by 3.1 km on average and 51.5% move up by 3.8 km.

[13] We also compute the local magnitude (M_L) for each event from seismogram maximum amplitudes, after converting signals to that expected for a Wood-Anderson instrument.

2.3. Uncertainty of Hypocenters

[14] Ninety percent of the formal (1-sigma) errors from single event location are 0.8–1.8 km horizontally and 0.7–2.0 km in depth. Formal errors of the deeper hypocenters (depth > 60 km) outside the MOOS network are 30% greater than for shallower earthquakes. To assess possible systematic bias in hypocenters, we test how much the locations move by increasing or decreasing P velocity by 0.25 km/s and S velocity by 0.15 km/s in each layer. These values correspond to the average change between our starting and final velocity model. For the earthquakes < 60 km deep, the depths shift about 3 km upward in the faster model and down in the slower model. The depth shifts of deeper earthquakes are also ~ 3 km while the epicenters shift about 9 km, two to three times larger than shallower earthquakes, resulting in a steepening in the dip of the WBZ (compare Figures 3c and 3d). Earthquakes west of the Kenai Peninsula beneath Cook Inlet, generally deeper than 60 km, lie outside the MOOS array. The raypaths of these deeper earthquakes travel within the downgoing slab to most stations, causing earthquakes to mislocate closer to the network due to shorter travel time [Hauksson, 1985]. Hence, the deeper (> 60 km) relocated hypocenters show steeper dip than the AEIC catalog, which should be more accurate for intermediate-depth earthquakes which are located outside the MOOS array but well within the AEIC network including some AVO stations (Figure 1).

[15] The hypocenters determined by hypoDD change in different velocity models by about 1 km for earthquakes 60 km deep, relative to changes in single event locations. However, if we use starting hypocenters for hypoDD initially located in the same faster or slower velocity model, the larger systematic shifts are preserved. Overall, systematic error due to velocity uncertainty in all hypocenters could be less than 3 km for shallower earthquakes, while the systematic errors for deeper earthquakes could be three times larger.

2.4. Focal Mechanisms

[16] We estimate fault-plane solutions from P wave first motions and SV/P and SH/P amplitude ratios for 117 microearthquakes, measured after FIR filter causality was corrected (supporting information Table S1). At least eight polarity and 16 SV/P or SH/P amplitude observations are used to constrain each focal mechanism. To reduce effects of higher-frequency scattering, amplitudes are measured in the 1 to 2 Hz frequency band, from the Hilbert-transform envelope of the signal in a window manually picked around the P or S wave. Amplitudes were also corrected for incidence angle and the free surface effect to give the amplitude expected for the incident P or S wave. Focal mechanism solutions are determined by grid search [Snoke, 2003] with angular 2.5° increments in strike, dip, and rake. For each earthquake, we trace rays to the stations in a piecewise-linear gradient velocity model adapted from our inverted velocity (Figure 2 and Table 2) and calculate the predicted amplitude ratios for each radiation pattern following standard methods [Aki and Richards, 2002]. Acceptable solutions are defined to include the least possible

Table 2. Velocity Model

Depth (km)	Final Vp (km/s)	Vp Uncertainty (2σ) (km/s)	Final Vs (km/s)	Vs Uncertainty (2σ) (km/s)
-1.0	4.08	0.094	3.02	0.056
0.5	6.06	0.023	3.49	0.008
15.0	6.31	0.015	3.61	0.006
30.0	6.95	0.008	3.91	0.004
45.0	7.77	0.007	4.34	0.004
70.0	8.56	0.016	4.84	0.006
110.0	8.78	0.064	4.85	0.029

number of incorrect polarity measurements (at most 2), and as few inconsistent amplitude ratios as possible, which is defined to be different greater than 4.0 compared with the predicted value. The value of 4.0 (implemented as $10^{0.6}$) was chosen by trial and error to eliminate data that fit poorly without throwing away most of the amplitude measurements. The focal mechanism that has the smallest standard deviation of the acceptable amplitude ratio differences between the prediction and observation is selected as the final solution. To quantify the uncertainty of the final solution, we calculate the uncertainty index U of Maeda [1992], which is defined as the root-mean-square of the angle of deviation of the null, P, and T axes between each acceptable focal mechanism and the best fitting one. We also track an aggregate observation error E as the sum of proportion of inconsistent observations for P polarity data and amplitude ratio data. Of the 117 focal mechanisms, 72 are assigned quality A, which have $U < 12^\circ$ and $E < 0.25$, and the rest are assigned quality B. The uncertainty in event depth and takeoff angle could add about 5–10° uncertainty to focal mechanism solution for events deeper than 20 km [Hardebeck and Shearer, 2002, 2003].

3. Results and Discussion

3.1. Relocation

[17] Relocated earthquakes are plotted in map view for several depth ranges. Figure 4a shows that seismicity

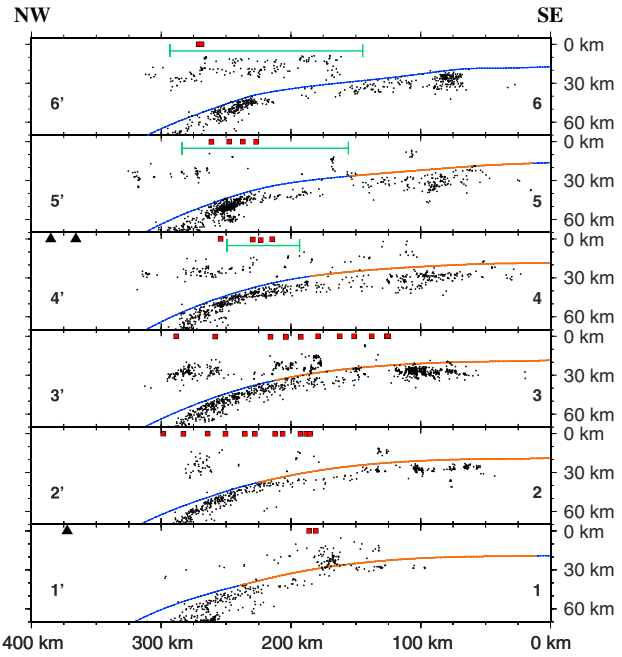


Figure 5. HypoDD locations projected on cross sections 1'-6' (see Figure 1 for locations). Solid line shows the plate interface, orange where it ruptured during the 1964 earthquake based on aftershocks [Sykes, 1971]. Green bar denotes the lateral extent of the slow-slip event region [Ohta et al., 2006]. Black triangles mark the locations of the active volcanoes. The red squares mark the locations of the MOOS network in the area.

shallower than 50 km is pervasive from the PWS to the Cook Inlet. Abundant seismicity occurs in the 1964 great earthquake rupture zone, concentrating in the PWS. Major terrane-boundary faults in the upper plate do not show clear lineations of microseismicity. Hypocenters in the WBZ (Figure 4b) increase in depth northward and steeply westward, defining the subducting slab. The decrease of

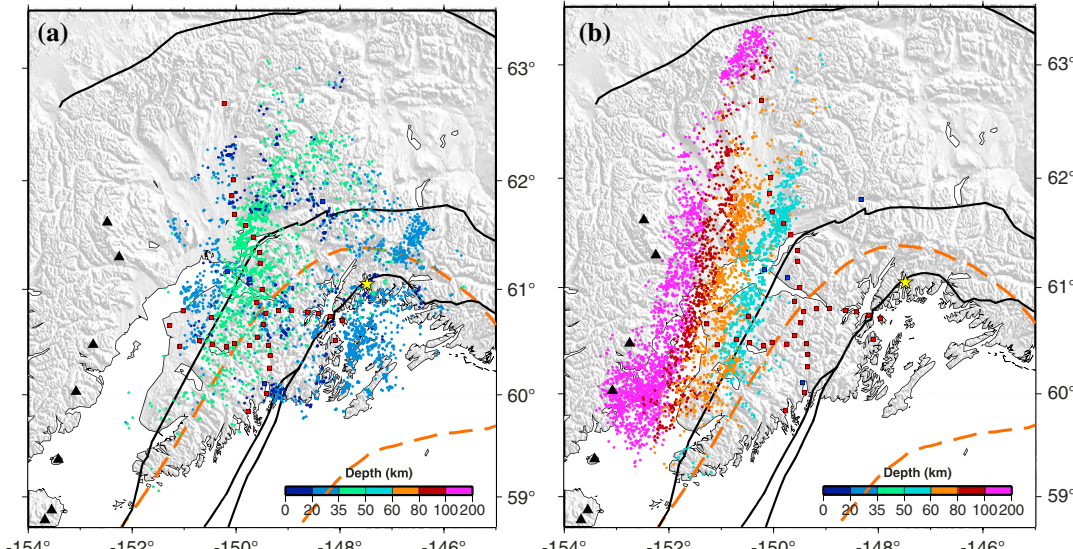


Figure 4. Map of hypoDD locations colored by different depth ranges, showing (a) earthquakes shallower than 50 km, and (b) earthquakes deeper than 50 km. Other symbols and lines are described in Figure 1.

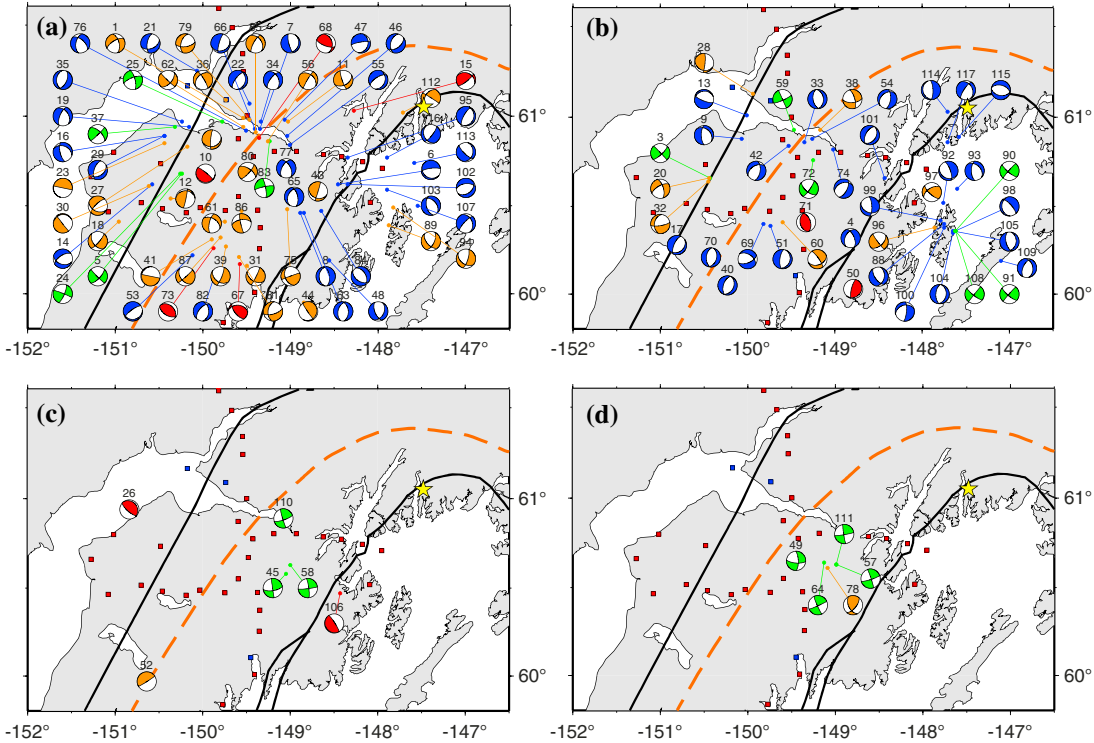


Figure 6. Focal mechanisms of 117 events. (a) Quality A events within downgoing slab. (b) Quality B events within downgoing slab. (c) Quality A events within overriding plate. (d) Quality B events within overriding plate. Focal mechanisms are sorted by faulting type by convention of *Frohlich* [1992]: Blue denotes normal faulting; Green denotes strike-slip; Red denotes thrusting-faulting; Orange shows none of the three typical faulting types.

seismicity north of 62°N could be related to the limit of detection of the MOOS network. However, the west-to-east termination of WBZ seismicity at 149°W – 150°W longitude is probably real, since numerous upper-plate earthquakes are successfully located further east. This termination indicates the eastern limit of the Aleutian WBZ.

[18] We show earthquakes in series of cross sections (Figure 5) to further investigate seismicity patterns and the shape of the subducting slab in shallower depth ($<50\text{ km}$). Cross sections 1–1' to 5–5' show earthquakes within 20 km distance from each projection line and are aligned with slab dip.

For reference, a plate interface surface (contours on Figure 1, lines on Figure 5) is mapped as a smooth surface immediately above all WBZ seismicity (determined by focal mechanism discussed in section 3.2) at 20 – 50 km depth, and following relocated AEIC seismicity [Ratchkovski and Hansen, 2002] deeper, where the WBZ lies outside the MOOS array. Upper-plate earthquakes occur in small clusters, many concentrating in northern Cook Inlet at around 20 km depth.

[19] By comparing the geometry of plate interface based on this seismicity with horizontal boundary of the inferred 1964 great earthquake rupture zone [Sykes, 1971], we infer

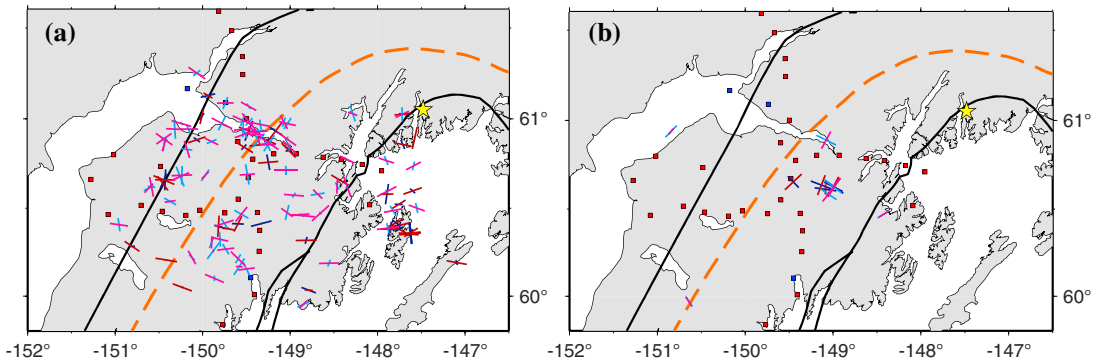


Figure 7. Map showing P and T axes of focal mechanisms in (a) downgoing slab, and (b) overriding plate. Short red lines in light and dark color are the T axes with quality A and quality B, respectively. Short blue lines in light and dark color are the P axes with quality A and quality B, respectively. Other symbols and lines are described in Figure 1.

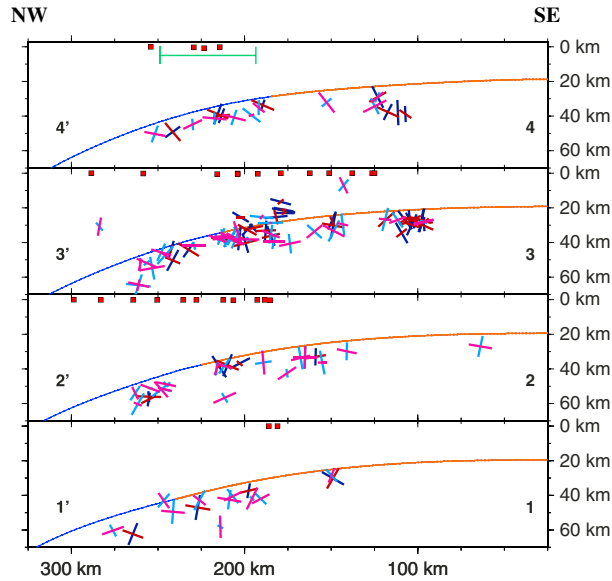


Figure 8. P and T axes of focal mechanisms projected on cross sections. Refer to Figures 5 and 7 for descriptions of lines and symbols.

that the depth of the downdip end of the seismogenic zone is at 30–40 km depth, consistent with thermal models [Oleskevich *et al.*, 1999] and geodetic inversions [Ohta *et al.*, 2006]. Abundant earthquakes in the 1964 rupture zone are consistently observed in cross sections. Cross section 6-6' is supposed to be outside of the 1964 rupture zone (orange line on Figure 1) but the seismicity pattern is not much different. Previous studies [Doser and Veilleux, 2009; Page *et al.*, 1989; Eberhart-Phillips *et al.*, 2006] show that the seismogenic zone seismicity is scattering in depth shallower than 40 km and could not distinguish the WBZ earthquakes from the overriding crustal earthquakes. Those earthquakes are located by a relatively sparse AEIC network and with velocity model averaged for a much broader region. With a

dense network, our seismicity clearly shows the geometry of the subducting slab in the seismogenic region.

3.2. Focal Mechanisms

[20] Among the 117 focal mechanisms we determined, 78 earthquakes lie within the 1964 earthquake rupture zone (Figure 6). Only seven are thrust faulting (Figures 6a and 6b), but their slip vectors are inconsistent with either the convergence direction or downdip direction. The focal mechanisms of earthquakes in the overriding plate and downgoing plate differ. In the overriding plate, a cluster of earthquakes is located in the middle of Kenai Peninsula between Border Range Fault and Contact Fault. These earthquakes have similar left-lateral strike-slip focal mechanisms, which could accommodate shearing in the overriding plate. In the downgoing slab, about 80% of the earthquakes shows normal faulting, for both quality A and B events.

[21] P and T axes of focal mechanisms are shown in a map view (Figure 7) and projected onto cross sections 1-1' to 4-4' (Figure 8). Focal mechanisms inside the downgoing slab and within the 1964 earthquake rupture zone show the P axes normal to the slab and the T axes following the slab dip direction rather than the relative plate motion direction (Figures 7, 8, and 9). In cross section 3-3', distinctive patterns of P and T axes help distinguish WBZ events from crustal events, constraining the location of the plate interface (Figure 8). The P and T axes for earthquakes outside the rupture zone show complex patterns (Figures 7, 8, and 9), possibly due to the rapid spatial stress change [Lu *et al.*, 1997]. Generally, the P and T axes directions of focal mechanisms agree with the local stress field inverted by Lu *et al.* [1997] in the same region. From the preponderance of normal-faulting focal mechanisms and the T axis directions, we speculate that the main stresses driving the intraslab earthquakes are related to slab bending or slab pull. The T axes are rotated somewhat more E-W than the downdip direction; possibly that is an influence of preexisting sea floor fabric. Magnetic anomalies are oriented roughly north-south in the Gulf of Alaska [Maus *et al.*, 2009], close to perpendicular to the dominant T axis

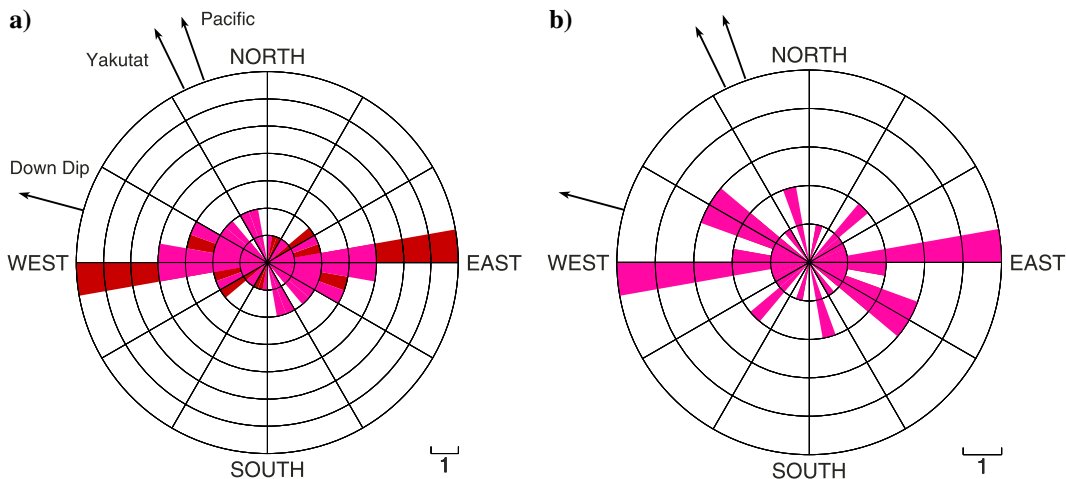


Figure 9. Rose histogram of T axes in the downgoing slab, excluding the ones with direction less than 15° from vertical. (a) Events within the 1964 earthquake rupture zone. (b) Events outside the 1964 rupture zone. Black arrows show the directions of Pacific plate motion, Yakutat terrane motion, and subducting slab downdip.

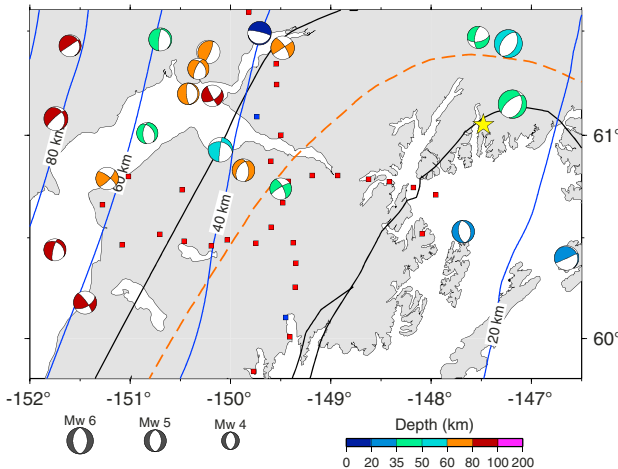


Figure 10. Focal mechanisms from the global CMT catalog since 1976 [Dziewonski *et al.*, 1981; Ekström *et al.*, 2012]. Event depth and magnitude are denoted by colors and size. Other symbols and lines are described in Figure 1.

orientation (Figure 9). In any case, the T axes of these normal faults do not align with plate motion so are unlikely to result from shear stresses between the plates, as would be expected if they indicated creep or a response to mechanical locking.

[22] Focal mechanisms from global-CMT catalog [Dziewonski *et al.*, 1981; Ekström *et al.*, 2012] since 1976 in the south-central Alaska are plotted in the same region (Figure 10). The majority of the large earthquakes ($M_w > 4.8$) exhibit normal and strike-slip faulting including the four events within the 1964 great

earthquake rupture zone. Thus, there is little evidence for thrust faulting along the thrust zone in the last 35 years.

3.3. Comparison With Structure

[23] Earthquakes projected on a nearby refraction line in PWS (Figure 1) are concentrated in the three subducting layers interpreted by Brocher *et al.* [1994] as Yakutat terrane over Pacific plate crust with sediments intervening (Figure 11a). In this interpretation, the earthquakes would lie below the top of the Yakutat terrane but within and above the underlying Pacific crust. However, it is unclear that this multilayer structure is required by the active-source data. A more recent wide-angle refraction/reflection study just to the east shows that the western Yakutat terrane is a more homogeneous body, with V_p increasing monotonically from 6.5 to 7.2 km/s in the lower 15–20 km below sediments with no internal layering, in contact with the Pacific lithosphere along a near-vertical fault [Christeson *et al.*, 2010; Worthington *et al.*, 2012]. The velocity structure compares favorably to those of oceanic plateaus. If all layers with $V_p = 6.0$ –7.2 km/s imaged by Brocher *et al.* [1994] corresponds to a thick oceanic plateau, then the seismicity all lies within subducting Yakutat terrane. Focal mechanisms also indicate that these earthquakes are within the subducting plate, in that they show downdip extension rather than thrust faulting, consistent with the active thrust fault lying above these layers.

[24] A scattered-wave migration image of dVs/Vs following profile 3-3' shows structure that agrees with the seismicity pattern quite well (Figure 11b). This image, discussed in a companion paper (Y. H. Kim *et al.*, Alaska Megathrust 2: Imaging the megathrust zone and Yakutat/Pacific plate interface in the

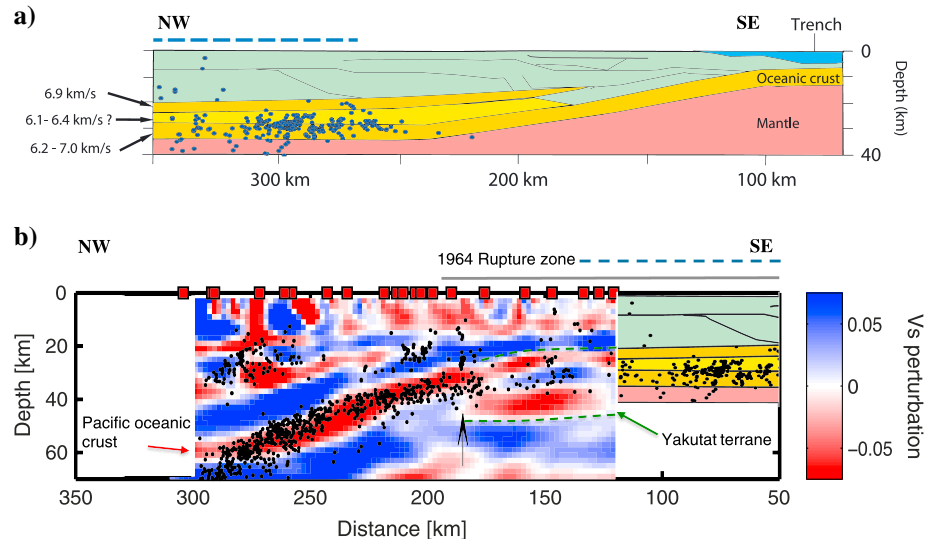


Figure 11. Comparison of hypocenters from MOOS with images in the Kenai. (a) Relocated earthquakes by hypoDD (dark blue dots) projected onto the TACT line [Brocher *et al.*, 1994]; location shown in Figure 1. The model includes seawater (light blue); deformed overriding crust (green); mantle (red). Yellow layers are interpreted by Brocher *et al.* [1994] as Yakutat terrane ($V_p = 6.9$ km/s layer), underlying sediments (6.1–6.4 km/s low-velocity zone), and subducting Pacific plate crust (6.2–7.0 km/s layer). Blue dashed line shows the overlapping part in Figures 11a and 11b. (b) Scattered-wave dVs/Vs image (AM2) for line 3-3' (Figure 1) with projected seismicity (black dots). Green dashed lines show the upper and lower boundaries of Yakutat terrane. Black arrow shows the boundary between the Pacific oceanic crust and the Yakutat terrane. TACT line is aligned with the east end of the image, for comparison.

Alaska subduction zone, submitted to *Journal of Geophysical Research: Solid Earth*, 2013) (hereinafter referred to as “AM2”), relies on data recorded by the same MOOS array. It shows a low-velocity layer thought to represent subducting crust, following the seismicity. The change in character underneath the central Kenai Peninsula may be the boundary between Pacific oceanic crust to the west and the Yakutat terrane to the east, the latter of which appears as a composite layer of two low-velocity zones with a high velocity zone in between, similar to the nearby active-source image [Brocher et al., 1994]. Seismicity deeper than 30 km depth lies within the low-velocity zone, interpreted as the subducting Pacific crust. At ~60 km depth, the seismicity band departs from the shallow-dipping low-velocity zone and dips more steeply. The deeper image may not reflect the real subducting structure and could be aliased by the thick sediment basin in Cook Inlet and lack of station coverage at the western end of MOOS array (AM2). In the shallower part and underneath the 1964 rupture zone, most earthquakes are within the upper Yakutat crust. Much of the upper-plate seismicity follows a low-velocity layer at 20–30 km depth, inferred to lie just above the downdip extent of the Contact Fault (AM2), perhaps within the Chugach Terrane thrust slice.

3.4. Megathrust Geometry

[25] All estimates to date of the seismic moment of the 1964 Alaska earthquake depend on different assumed geometries of faulting during the earthquake, which vary from 6° to 20° in dip [Christensen and Beck, 1994; Ichinose et al., 2007; Johnson et al., 1996; Kanamori, 1970; Stauber and Bollinger, 1966]. In this study, focal mechanisms confirm the continuous narrow band of seismicity to be within the subducting structure, which is interpreted as the 15–20 km thick Yakutat terrane. Thus, the megathrust lies on top of the subducting Yakutat terrane, with dip angle about 3°. This is significantly shallower than the dip assumed in previous rupture models, and could lead to significant seismic moment underestimates, because some vertical elements of the source excitation function are proportional to sine of the dip. The shallower dip could explain the 50% difference in seismic moment between some tsunami- and geodetic-based estimates [Ichinose et al., 2007] and long-period surface-wave based estimates [Kanamori, 1977], favoring the latter.

3.5. Interplate Thrust Zone Earthquakes

[26] Most subduction zones exhibit interplate earthquakes on the megathrust faults [e.g., Ekström et al., 2012; Pacheco and Sykes, 1992; Ruff and Kanamori, 1980]. In a few regions currently in the interseismic interval of giant earthquakes (Southern Chile [Dzierma et al., 2012], Southwest Japan [Obana et al., 2004], Cascadia [Wada et al., 2010; McCrory et al., 2012]), even small thrust earthquakes are absent. In these places, clusters of small earthquakes frequently occur adjacent to the seismogenic zone but within the downgoing plate, with focal mechanisms similar to deeper WBZ seismicity. In Alaska, we clearly observe a well-defined seismic zone that parallels the thrust zone but shows no thrust faulting even at magnitudes below 1.0; we infer that these earthquakes lie just below the plate boundary for reasons outlined above. These regions, including south Alaska, share some common features, such as thick trench sediment (>1 km) [Heuret et al., 2012], long interseismic

cycle (>> 100 years) [Goes, 1996], and large areas of the locked plate interface [Liu et al., 2010; Mazzotti et al., 2003; Moreno et al., 2011].

[27] The presence or absence of small-to-moderate interplate thrust earthquakes in the seismogenic region could be related to stages of seismic cycle. It has been noticed that the rupture zone for major earthquake enters a period of relative quiescence after the aftershock sequence ends [Mogi, 1979; Pérez and Scholz, 1997]. In addition, temporal variation of the stress field for regions updip and downdip of the seismogenic zone is indicated by changes of outer-rise and intermediate-depth earthquake focal mechanisms before and after giant megathrust earthquakes [Christensen and Ruff, 1988; Dmowska et al., 1988]. The stress accumulation along the locked plate interface during seismic cycle should also vary. For data presented here, it has been 43 years (1964–2007) since the last great earthquake, a small fraction of the 333–875 year recurrence time [Carver and Plafker, 2008]. Possibly, the thrust faulting has not returned to the seismogenic zone because the 1964 earthquake released much stress, and shear stresses remain far from failure.

[28] This effect could be enhanced by a relatively smooth plate interface, since material properties in the seismogenic zone could also affect the seismic behavior of interplate thrust fault. It has been noticed that accretionary wedges with abundant sediment input are more capable of generating giant earthquakes [Bilek, 2010; Heuret et al., 2012]. The Yakutat terrane is covered by ~10 km thick sediments offshore [Worthington et al., 2012], and while much may be offscraped, a 2 km thick layer of sediments may have been subducted with the Yakutat terrane [Griscom and Sauer, 1990; Plafker, 1987]. The thick subducted sediments should create a homogeneous and coherent contact zone on the plate interface [Ruff, 1989; Tanioka et al., 1997]. Studies of the moment release for the 1964 earthquake indicate the existence of a large patch in eastern Kenai Peninsula and PWS [Ruff and Kanamori, 1983], where most of the moment is released [e.g., Christensen and Beck, 1994; Johnson et al., 1996]. Thus, small heterogeneities, which could nucleate smaller earthquakes, may be absent. It has been proposed that smaller irregularities on the seafloor like seamounts may cause high-slip rupture over an area similar to their size once subducted [Estabrook et al., 1994; Bilek et al., 2003; Das and Watts, 2009]. Such features seem absent within the exposed Yakutat terrane, whose subducted portion underlies the large PWS asperity. Perhaps the locked plate interface is homogenous with respect to unstable seismic sliding, so that earthquakes can only happen when the megathrust ruptures as a whole.

[29] The early stage in seismic cycle and smoothness of subducting slab surface are not independent factors, but could jointly contribute to the lack of thrust earthquakes in the seismogenic zone. A relatively smooth surface may take a longer time for tectonic loading to start producing interplate earthquakes than a rough one, because small heterogeneities that could serve as stress concentrators are absent. Our study shows that the large asperity that produced much of the coseismic slip during 1964 Alaska earthquake is completely aseismic in the early stage of seismic cycle. To better understand how plate interface roughness affects the presence of interplate thrust earthquake during the interseismic cycle, we need more observations from thrust zones in different stages of the seismic cycle and with different plate roughness characteristics.

4. Conclusions

[30] In south-central Alaska, the MOOS array recorded over 12,000 local earthquakes in 13 months. Relocation of 8308 hypocenters shows that seismicity is pervasive within the rupture zone of 1964 great earthquake. However, none of the seismicity is due to thrust faulting on the plate boundary, but shows deformation within the downgoing plate. Cross sections of seismicity clearly show the geometry of the plate interface; it lies between Yakutat terrane and North America plate at 20 km to 40 km depth and dips at 3° through much of the thrust zone. Most microearthquakes are showing normal faulting mechanisms, and the direction of the T axes generally follows the dipping direction of the slab, indicating that they lie inside the subducting slab under downdip extension or result from plate bending. The fact that interplate thrust events are absent could indicate little stress accumulation since 1964 great earthquake relative to that accumulated over a full seismic cycle. Also, perhaps the Yakutat terrane together with thick overlying sediments forms a large homogeneous contact zone, preventing the interface from sliding seismically except during great earthquakes.

[31] **Acknowledgments.** This project was supported by NSF grants EAR-0814235 (Abers) and EAR-0409950 (Christensen). Y. Kim was supported by the Korea Meteorological Administration Research and Development Program under grant CATER-2013-8010. We thank the many people who contributed to collecting the MOOS data set, in particular J. Brewer, J. Elliott, A. Foster, J. Freymueller, K. Godfrey, S. Hansson, A. Perttu, M. Thorne, Z. Zhang, and the staff of the IRIS-PASSCAL Instrument Center. Associate Editor R. Nowack and two anonymous reviewers made excellent suggestions to improve the manuscript. J. Calkins contributed to early phases of this analysis. Most figures were made using GMT [Wessel and Smith, 1991].

References

- Abers, G. A., and S. W. Roecker (1991), Deep structure of an arc-continent collision: earthquake relocation and inversion for upper mantle P and S wave velocities beneath Papua New Guinea, *J. Geophys. Res.*, 96(B4), 6379–6401.
- Aki, K., and P. G. Richards (2002), *Quantitative Seismology Theory and Methods*, 2nd ed., 704 pp., Univ. Sci. Books, Sausalito, Calif.
- Allen, R. V. (1978), Automatic earthquake recognition and timing from single traces, *Bull. Seismol. Soc. Am.*, 68(5), 1521–1532.
- Bilek, S. L., S. Y. Schwartz, and H. R. DeShon (2003), Control of seafloor roughness on earthquake rupture behavior, *Geology*, 31(5), 455–458.
- Bilek, S. L. (2010), The role of subduction erosion on seismicity, *Geology*, 38(5), 479–480.
- Brocher, T. M., G. S. Fuis, M. A. Fisher, G. Plafker, M. J. Moses, J. J. Taber, and N. I. Christensen (1994), Mapping the Megathrust beneath the Northern Gulf of Alaska Using Wide-Angle Seismic Data, *J. Geophys. Res.*, 99(B6), 11,663–11,685.
- Byrne, D. E., D. M. Davis, and L. R. Sykes (1988), Loci and maximum size of thrust earthquakes and the mechanics of the shallow region of subduction zones, *Tectonics*, 7(4), 833–857.
- Brunn, T. R. (1983), Model for the origin of the Yakutat block, an accreting terrane in the northern Gulf of Alaska, *Geology*, 11(12), 718–721.
- Carver, G., and G. Plafker (2008), Paleoseismicity and neotectonics of the Aleutian subduction zone—an overview, in *Active Tectonics and Seismic Potential of Alaska*, Geoph. Monog. Series, vol. 179, pp. 43–63, AGU, Washington, D. C.
- Christensen, D. H., and L. J. Ruff (1988), Seismic coupling and outer rise earthquakes, *J. Geophys. Res.*, 93(B11), 13,421–13,444.
- Christensen, D. H., and S. L. Beck (1994), The Rupture Process and Tectonic Implications of the Great 1964 Prince William Sound Earthquake, *Pure Appl. Geophys.*, 142(1), 29–53.
- Christeson, G. L., S. P. S. Gulick, H. J. A. van Avendonk, L. L. Worthington, R. S. Reece, and T. L. Pavlis (2010), The Yakutat terrane: Dramatic change in crustal thickness across the Transition fault, Alaska, *Geology*, 38(10), 895–898.
- Das, S., and A. B. Watts (2009), Effect of subducting seafloor topography on the rupture characteristics of great subduction zone earthquakes, in *Subduction Zone Geodynamics*, edited by S. Lallemand and F. Funiciello, Springer-Verlag, Berlin, Heidelberg, pp. 103–118.
- Dmowska, R., J. R. Rice, L. C. Lovison, and D. Josell (1988), Stress transfer and seismic phenomena in coupled subduction zones during the earthquake cycle, *J. Geophys. Res.*, 93(B7), 7869–7884.
- Doser, D. I., and A. M. Veilleux (2009), A Comprehensive Study of the Seismicity of the Kenai Peninsula–Cook Inlet Region, South-Central Alaska, *Bull. Seismol. Soc. Am.*, 99(4), 2208–2222.
- Dzierna, Y., M. Thorwart, W. Rabbel, C. Siegmund, D. Comte, K. Bataille, P. Iglesia, and C. Prezzi (2012), Seismicity near the slip maximum of the 1960 Mw 9.5 Valdivia earthquake (Chile): Plate interface lock and reactivation of the subducted Valdivia Fracture Zone, *J. Geophys. Res.*, 117, B06312, doi:10.1029/2011JB008914.
- Dziewonski, A., T. A. Chou, and J. Woodhouse (1981), Determination of earthquake source parameters from waveform data for studies of global and regional seismicity, *J. Geophys. Res.*, 86(B4), 2825–2852.
- Eberhart-Phillips, D., D. H. Christensen, T. M. Brocher, R. Hansen, N. A. Ruppert, P. J. Haessler, and G. A. Abers (2006), Imaging the transition from Aleutian subduction to Yakutat collision in central Alaska, with local earthquakes and active source data, *J. Geophys. Res.*, 111, B11303, doi:10.1029/2005JB004240.
- Ekström, G., M. Nettles, and A. M. Dziewoński (2012), The global CMT project 2004–2010: Centroid-moment tensors for 13,017 earthquakes, *Phys. Earth Planet. Inter.*, 200–201, 1–9.
- Elliott, J. L., C. F. Larsen, J. T. Freymueller, and R. J. Motyka (2010), Tectonic block motion and glacial isostatic adjustment in southeast Alaska and adjacent Canada constrained by GPS measurements, *J. Geophys. Res.*, 115, B09407, doi:10.1029/2009JB007139.
- Estabrook, C. H., K. H. Jacob, and L. R. Sykes (1994), Body wave and surface wave analysis of large and great earthquakes along the Eastern Aleutian Arc, 1923–1993: Implications for future events, *J. Geophys. Res.*, 99(B6), 11,643–11,662.
- Ferris, A., G. A. Abers, D. H. Christensen, and E. Veenstra (2003), High resolution image of the subducted Pacific (?) plate beneath central Alaska, 50–150 km depth, *Earth Planet. Sci. Lett.*, 214(3–4), 575–588.
- Frohlich, C. (1992), Triangle diagrams: ternary graphs to display similarity and diversity of earthquake focal mechanisms, *Phys. Earth Planet. Inter.*, 75(1), 193–198.
- Goes, S. D. B. (1996), Irregular recurrence of large earthquakes: an analysis of historic and paleoseismic catalogs, *J. Geophys. Res.*, 101(B3), 5739–5749.
- Griscom, A., and P. E. Sauer (1990), Interpretation of magnetic maps of the northern Gulf of Alaska, with emphasis on the source of the Slope anomaly, *U.S. Geol. Surv. Open File Rep.* 90-348, 18 pp.
- Hardebeck, J. L., and P. M. Shearer (2002), A new method for determining first-motion focal mechanisms, *Bull. Seismol. Soc. Am.*, 92(6), 2264–2276.
- Hardebeck, J. L., and P. M. Shearer (2003), Using S/P amplitude ratios to constrain the focal mechanisms of small earthquakes, *Bull. Seismol. Soc. Am.*, 93(6), 2434–2444.
- Hauksson, E. (1985), Structure of the Benioff Zone Beneath the Shumagin Islands, Alaska: Relocation of Local Earthquakes Using Three-Dimensional Ray Tracing, *J. Geophys. Res.*, 90(B1), 635–649.
- Heuret, A., C. Conrad, F. Funiciello, S. Lallemand, and L. Sandri (2012), Relation between subduction megathrust earthquakes, trench sediment thickness and upper plate strain, *Geophys. Res. Lett.*, 39, L05304, doi:10.1029/2011GL050712.
- Ichinose, G., P. Somerville, H. K. Thio, R. Graves, and D. O’Connell (2007), Rupture process of the 1964 Prince William Sound, Alaska, earthquake from the combined inversion of seismic, tsunami, and geodetic data, *J. Geophys. Res.*, 112, B07306, doi:10.1029/2006JB004728.
- Igarashi, T., T. Matsuzawa, and A. Hasegawa (2003), Repeating earthquakes and interplate aseismic slip in the northeastern Japan subduction zone, *J. Geophys. Res.*, 108(B5), 2249, doi:10.1029/2002JB001920.
- Johnson, J. M., K. Satake, S. R. Holdahl, and J. Sauber (1996), The 1964 Prince William Sound earthquake: Joint inversion of tsunami and geodetic data, *J. Geophys. Res.*, 101(B1), 523–532.
- Kanamori, H. (1970), The Alaska earthquake of 1964: Radiation of long-period surface waves and source mechanism, *J. Geophys. Res.*, 75(26), 5029–5040.
- Kanamori, H. (1977), The energy release in great earthquakes, *J. Geophys. Res.*, 82(20), 2981–2987.
- Kennett, B., and E. Engdahl (1991), Traveltimes for global earthquake location and phase identification, *Geophys. J. Int.*, 105(2), 429–465.
- Lay, T., H. Kanamori, and L. Ruff (1982), The Asperity Model and the Nature of Large Subduction Zone Earthquakes, *Earthquake Pred. Res.*, 1(1), 3–71.
- Lay, T., L. Astiz, H. Kanamori, and D. H. Christensen (1989), Temporal Variation of Large Intraplate Earthquakes in Coupled Subduction Zones, *Phys. Earth Planet. Inter.*, 54(3–4), 258–312.
- Lay, T., and S. Bilek (2007), Anomalous earthquake ruptures at shallow depths on subduction zone megathrusts, in *The Seismogenic Zone of Subduction Zone Thrust Faults*, MARGINS Theor. Experim. Earth Sci. Ser., edited by T. H. Dixon and J. C. Moore, pp. 476–511, Columbia Univ. Press, New York.

- Liu, Z., S. Owen, D. Dong, P. Lundgren, F. Webb, E. Hetland, and M. Simons (2010), Estimation of interplate coupling in the Nankai trough, Japan using GPS data from 1996 to 2006, *Geophys. J. Int.*, 181(3), 1313–1328.
- Lu, Z., M. Wyss, and H. Pulpan (1997), Details of stress directions in the Alaska subduction zone from fault plane solutions, *J. Geophys. Res.*, 102(B3), 5385–5402.
- Maeda, N. (1992), A method of determining focal mechanisms and quantifying the uncertainty of the determined focal mechanisms for microearthquakes, *Bull. Seismol. Soc. Am.*, 82(6), 2410–2429.
- Maus, S., et al. (2009), EMAG2: A 2-arc min resolution Earth Magnetic Anomaly Grid compiled from satellite, airborne, and marine magnetic measurements, *Geochem. Geophys. Geosyst.*, 10, Q08005, doi:10.1029/2009GC002471.
- Mazzotti, S., H. Dragert, J. Henton, M. Schmidt, R. Hyndman, T. James, Y. Lu, and M. Craymer (2003), Current tectonics of northern Cascadia from a decade of GPS measurements, *J. Geophys. Res.*, 108(B12), 2554, doi:10.1029/2003JB002653.
- McCrory, P. A., J. L. Blair, F. Waldhauser, and D. H. Oppenheimer (2012), Juan de Fuca slab geometry and its relation to Wadati-Benioff zone seismicity, *J. Geophys. Res.*, 117, B09306, doi:10.1029/2012JB009407.
- Mogi, K. (1979), Two kinds of seismic gaps, *Pure Appl. Geophys.*, 117(6), 1172–1186.
- Moreno, M., D. Melnick, M. Rosenau, J. Bolte, J. Klotz, H. Echtler, J. Baez, K. Bataille, J. Chen, and M. Bevis (2011), Heterogeneous plate locking in the South-Central Chile subduction zone: Building up the next great earthquake, *Earth Planet. Sci. Lett.*, 305(3), 413–424.
- Obana, K., S. Kodaira, and Y. Kaneda (2004), Microseismicity around rupture area of the 1944 Tonankai earthquake from ocean bottom seismograph observations, *Earth Planet. Sci. Lett.*, 222(2), 561–572.
- Ohta, Y., J. T. Freymueller, S. Hreinsdóttir, and H. Suito (2006), A large slow slip event and the depth of the seismogenic zone in the south central Alaska subduction zone, *Earth Planet. Sci. Lett.*, 247(1), 108–116.
- Oleskevich, D., R. Hyndman, and K. Wang (1999), The updp and downdip limits to great subduction earthquakes: thermal and structural models of Cascadia, south Alaska, SW Japan, and Chile, *J. Geophys. Res.*, 104(B7), 14,965–14,991.
- Pacheco, J. F., and L. R. Sykes (1992), Seismic moment catalog of large shallow earthquakes, 1900 to 1989, *Bull. Seismol. Soc. Am.*, 82(3), 1306–1349.
- Pacheco, J. F., L. R. Sykes, and C. H. Scholz (1993), Nature of seismic coupling along simple plate boundaries of the subduction type, *J. Geophys. Res.*, 98(B8), 14,133–14,159.
- Page, R. A., C. D. Stephens, and J. C. Lahr (1989), Seismicity of the Wrangell and Aleutian Wadati-Benioff zones and the North American plate along the Trans-Alaska crustal transect, Chugach Mountains and Copper River basin, southern Alaska, *J. Geophys. Res.*, 94(B11), 16,059–16,082.
- Pavlis, G. L., and J. R. Booker (1980), The mixed discrete-continuous inverse problem: application to the simultaneous determination of earthquake hypocenters and velocity structure, *J. Geophys. Res.*, 85(B9), 4801–4810.
- Pérez, O. J., and C. H. Scholz (1997), Long-term seismic behavior of the focal and adjacent regions of great earthquakes during the time between two successive shocks, *J. Geophys. Res.*, 102(B4), 8203–8216.
- Pisarenko, V. F., A. F. Kushnir, and I. V. Savin (1987), Statistical Adaptive Algorithms for Estimation of Onset Moments of Seismic Phases, *Phys. Earth Planet. Inter.*, 47, 4–10.
- Plafker, G. (1965), Tectonic Deformation Associated with the 1964 Alaska Earthquake The earthquake of 27 March 1964 resulted in observable crustal deformation of unprecedented areal extent, *Science*, 148(3678), 1675–1687.
- Plafker, G. (1987), Regional geology and petroleum potential of the northern Gulf of Alaska continental margin, in *Geology and Resource Potential of the Continental Margin of Western North America and Adjacent Ocean Basins*, Circum-Pacific Council for Energy and Mineral Resources, Earth Science Series, vol. 6, edited by D. W. Scholl, A. Grantz, and J. G. Vedder, pp. 229–268, Circum-Pacific Council for Energy and Mineral Resources, Houston, Texas.
- Plafker, G., J. C. Moore, and G. R. Winkler (1994), Geology of the southern Alaska margin, in *The Geology of Alaska, The Geology of North America*, vol. G-1, edited by G. Plafker and H. C. Berg, pp. 389–449, Geol. Soc. Am., Boulder, Colo.
- Ratchkovski, N. A., and R. A. Hansen (2002), New evidence for segmentation of the Alaska subduction zone, *Bull. Seismol. Soc. Am.*, 92(5), 1754–1765.
- Ruff, L., and H. Kanamori (1980), Seismicity and the subduction process, *Phys. Earth Planet. Inter.*, 23(3), 240–252.
- Ruff, L., and H. Kanamori (1983), The rupture process and asperity distribution of three great earthquakes from long-period diffracted P-waves, *Phys. Earth Planet. Inter.*, 31(3), 202–230.
- Ruff, L. (1989), Do trench sediments affect great earthquake occurrence in subduction zones?, *Pure Appl. Geophys.*, 129(1), 263–282.
- Scherbaum, F., and M. P. Bouin (1997), FIR filter effects and nucleation phases, *Geophys. J. Int.*, 130(3), 661–668.
- Snoke, J. A. (2003), 85.12 FOCMEC: FOCal MEchanism Determinations, *Int. Geophys.*, 81, 1629–1630.
- Stauder, W., and G. Bollinger (1966), The focal mechanism of the Alaska earthquake of March 28, 1964, and of its aftershock sequence, *J. Geophys. Res.*, 71(22), 5283–5296.
- Suito, H., and J. T. Freymueller (2009), A viscoelastic and afterslip postseismic deformation model for the 1964 Alaska earthquake, *J. Geophys. Res.*, 114, B11404, doi:10.1029/2008JB005954.
- Sykes, L. R. (1971), Aftershock zones of great earthquakes, seismicity gaps, and earthquake prediction for Alaska and the Aleutians, *J. Geophys. Res.*, 76(32), 8021–8041.
- Taber, J. J., and S. W. Smith (1985), Seismicity and focal mechanisms associated with the subduction of the Juan de Fuca plate beneath the Olympic Peninsula, Washington, *Bull. Seismol. Soc. Am.*, 75(1), 237–249.
- Tanioka, Y., L. Ruff, and K. Satake (1997), What controls the lateral variation of large earthquake occurrence along the Japan Trench?, *Isl. Arc.*, 6(3), 261–266.
- Thatcher, W. (1990), Order and diversity in the modes of Circum-Pacific Earthquake recurrence, *J. Geophys. Res.*, 95(B3), 2609–2623.
- Tichelar, B. W., and L. J. Ruff (1993), Depth of seismic coupling along subduction zones, *J. Geophys. Res.*, 98(B2), 2017–2037.
- Veilleux, A. M., and D. I. Doser (2007), Studies of Wadati-Benioff zone seismicity of the Anchorage, Alaska, region, *Bull. Seismol. Soc. Am.*, 97(1B), 52–62.
- Wada, I., S. Mazzotti, and K. L. Wang (2010), Intraslab Stresses in the Cascadia Subduction Zone from Inversion of Earthquake Focal Mechanisms, *Bull. Seismol. Soc. Am.*, 100(5A), 2002–2013.
- Waldhauser, F., and W. L. Ellsworth (2000), A double-difference earthquake location algorithm: method and application to the northern Hayward fault, California, *Bull. Seismol. Soc. Am.*, 90(6), 1353–1368.
- Wessel, P., and W. H. Smith (1991), Free software helps map and display data, *EOS Trans. AGU*, 72(41), 441–446.
- Worthington, L. L., H. J. A. Van Avendonk, S. P. S. Gulick, G. L. Christeson, and T. L. Pavlis (2012), Crustal structure of the Yakutat terrane and the evolution of subduction and collision in southern Alaska, *J. Geophys. Res.*, 117, B01102, doi:10.1029/2011JB008493.
- Zhang, Z., and S. Y. Schwartz (1992), Depth distribution of moment release in underthrusting earthquakes at subduction zones, *J. Geophys. Res.*, 97(B1), 537–544.
- Zweck, C., J. T. Freymueller, and S. C. Cohen (2002), Three-dimensional elastic dislocation modeling of the postseismic response to the 1964 Alaska earthquake, *J. Geophys. Res.*, 107(B4), 2064, doi:10.1029/2001JB000409.